Regular Article

A cuboidal B2 nanoprecipitation-enhanced body-centered-cubic alloy Al$_{0.7}$CoCrFe$_2$Ni with prominent tensile properties

Qing Wang [a,*], Yue Ma [a], Beibei Jiang [a], Xiaona Li [a], Yao Shi [a], Chuang Dong [a], Peter K. Liaw [b,*]

[a] Key Laboratory of Materials Modification by Laser, Ion and Electron Beams (Ministry of Education), School of Materials Science and Engineering, Dalian University of Technology, Dalian 116024, China
[b] Department of Materials Science and Engineering, The University of Tennessee, Knoxville, TN 37996, USA

ABSTRACT

The present work reports a cuboidal B2-coherently-enhanced body-centered-cubic (BCC) alloy Al$_{0.7}$CoCrFe$_2$Ni with prominent tensile properties at both room (ultimate tensile strength σ_b = 1223 MPa and elongation to fracture δ = 7.9%) and high temperatures. This multi-principal-element alloy is developed out of a cluster formula [Al–M$_{14}$]Al$_1$ issued from the cluster-plus-glue-atom model of a BCC structure. Here, the [Al–M$_{14}$] cluster is centered by Al, surrounded by fourteen average atoms M = Co$_{1/5}$Cr$_{1/5}$Fe$_{2/5}$Ni$_{1/5}$, and glued with one Al atom. Its excellent mechanical properties are attributed to a superalloy-like microstructure, characterized by cuboidal B2 nanoprecipitates coherently embedded in the BCC matrix.

© 2016 Elsevier Ltd. All rights reserved.

High strengths of metallic alloys, especially at high temperatures, rely mainly on precipitation hardening. The size, morphology, coherency, and distribution of secondary precipitates all contribute to mechanical behaviors. The most well-known example is Ni-base superalloys, which is characterized by cuboidal γ′ nanoprecipitates with a L1$_2$ structure (Cu$_3$Au-type) embedded coherently in the face-centered-cubic (FCC) γ matrix [1]. However, the precipitation hardening by the body-centered-cubic (BCC) ordered phases, such as a B2 phase (CsCl-type), in the BCC matrix generally deteriorates the ductility sharply [2]. This embrittlement is even more pronounced in multi-principal-element alloys (also popularly called high entropy alloys) containing Al and transition metals (TMs) [3–7]. Despite of their excellent properties, such as high-temperature structural stabilities, corrosion- and oxidation-resistances, their potential applications have been hindered by lack of ductility in BCC-based alloys and by low strength in FCC ones [8–13]. For instance, with increasing the Al content, the structures of the Al$_x$CoCrFeNi (molar ratio) alloy series would change gradually from FCC (x ≤ 0.45) to BCC plus B2 phases (x ≥ 0.88) [8]. At room temperature, an FCC Al$_{0.3}$CoCrFeNi alloy exhibits a good tensile ductility but suffers from a low yielding strength below 200 MPa [9], while the yielding strength of the cold-rolled Al$_{0.5}$CoCrFeNiCu alloy could be improved up to 1284 MPa as a result of nano-sized L1$_2$-γ′ precipitates coherently embedded in FCC-γ matrix [10]. In contrast, the BCC AlCoCrFeNi alloy, containing a richer Al content, is hard and brittle due to a spinodal

microstructure of BCC and B2 [11,12]. It is anticipated, therefore, that a BCC-based Al–TM multi-principal-element alloy, strengthened by coherent precipitation hardening, just like γ′ in γ, might show both high strength and good ductility.

The control of such a type of microstructure would require that the alloy reaches the lower limit for the BCC stabilization and contains certain elements favoring the formation of a BCC-ordered phase. With regards to the latter point, many BCC ordered phases, such as B2-AlTM, tends to form in Al–TM multi-element systems. The phase stability ranges for Al–TM multi-principal-element alloys are also roughly known, which has been correlated with a valence electron concentration parameter VEC, i.e., VEC ≥ 8.0 for FCC, 6.87 ≤ VEC < 8.0 for FCC plus BCC, and VEC < 6.87 for BCC plus B2 [14]. However, these phase-zone boundaries are not clearly defined because both the Al content and the different TM combinations contribute to the phase stabilities. A structural model is, therefore, required to describe accurately the structure stability state at each critical limit.

It is widely accepted that solid solutions are characterized by chemical short-range ordering [15,16], i.e., certain inter-atomic neighboring tendencies are developed that leads to local structural heterogeneities with respect to the average structure. Pronounced Al–TM nearest-neighbor atomic pairs have been unveiled in an Al$_{1.3}$CoCrCuFeNi multi-principal element alloy by neutron diffraction [17]. A new structural approach, the cluster-plus-glue-atom model [18], was recently introduced to address the structural modeling of solid solutions. In this model, any chemical short-range order is idealized into a local nearest-neighbor coordination polyhedral cluster and the sites in-

* Corresponding authors.
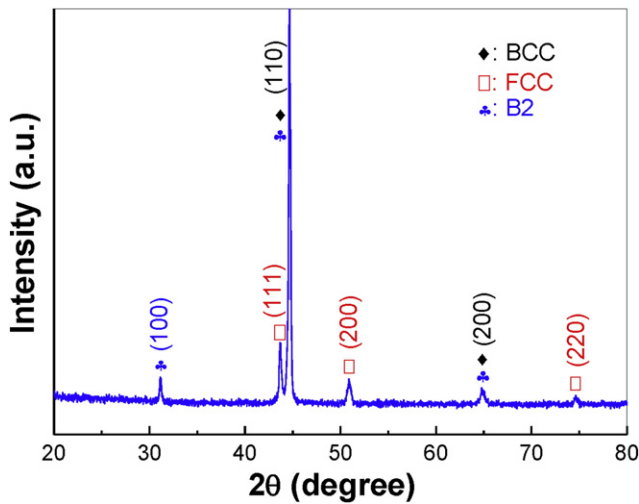 E-mail addresses: wangq@dlut.edu.cn (Q. Wang), pliaw@utk.edu (P.K. Liaw).

Fig. 1. XRD pattern of the suction-cast $Al_{0.7}CoCrFe_2Ni$ multi-principal-element alloy.

zero tensile ductility due to a BCC plus B2 spinodal-type microstructure [12].

The alternative way is to adjust the TM combinations by adding more elements with lower VEC values. So, in the present work, an average element, $M = Co_{1/5}Cr_{1/5}Fe_{2/5}Ni_{1/5}$, is attempted, in which the VEC is 8.2, slightly lower than 8.25 of the equi-molar $M = Co_{1/4}Cr_{1/4}Fe_{1/4}Ni_{1/4}$. Thus, the designed alloy $[Al–M_{14}]Al_1$ ($M = Co_{1/5}Cr_{1/5}Fe_{2/5}Ni_{1/5}$, $Al_{12.5}Co_{17.5}Cr_{17.5}Fe_{35}Ni_{17.5}$ at.%), abbreviated as $Al_{0.7}CoCrFe_2Ni$, has a lower VEC of 7.55 and should show an enhanced BCC structural stability. Moreover, since this VEC value is still largely above 6.87 (the upper VEC
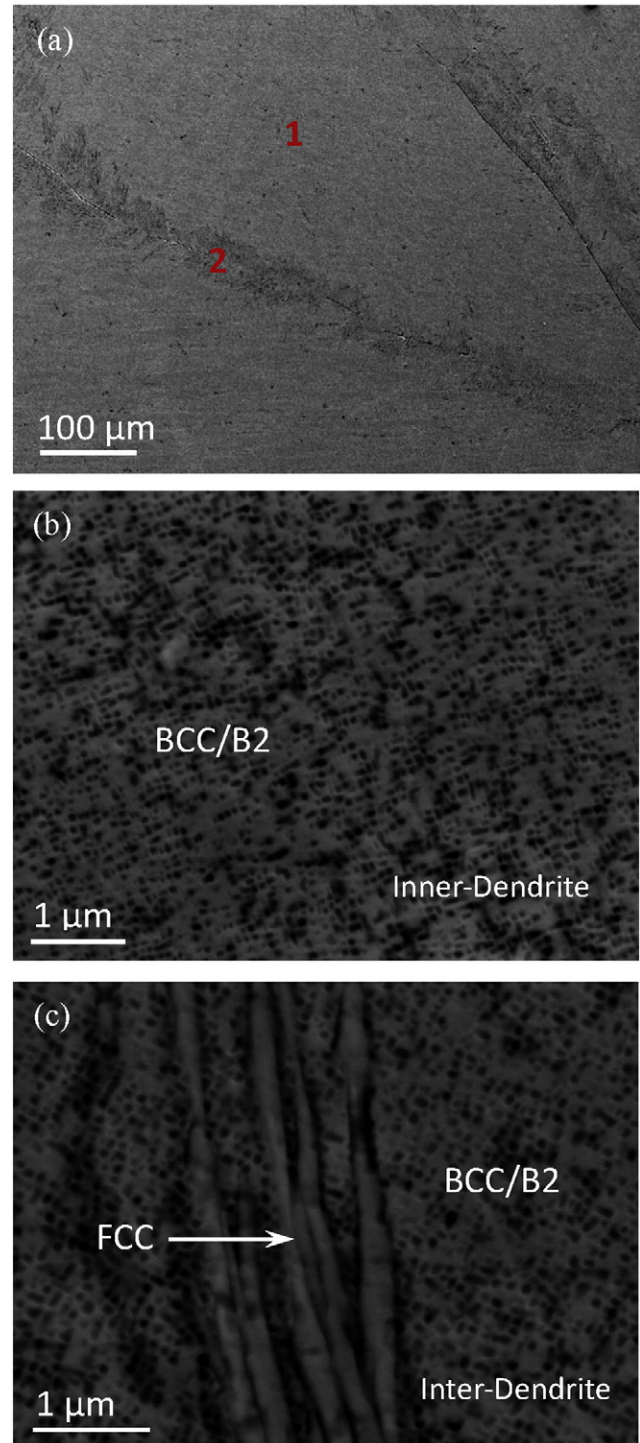
between the clusters are filled with glue atoms, which could be expressed with a composition formula of [cluster](glue atoms)$_x$ (x is the glue atom number for matching one cluster). There exist three types of atom sites, i.e., the cluster center, the cluster shell, and the glue sites, where the atomic occupancies in these three sites are determined by the enthalpies of mixing (ΔH) representing atomic interactions between the solute elements and the base solvent one. A solute showing a negative ΔH tends to occupy the cluster center and then the glue site, and that showing a weak ΔH tends to take the glue site. Such a cluster-based formulism has been validated in a variety of FCC and BCC alloys [18,19], confirming that widely-used alloys generally satisfy a limited number of specific composition formulas. Taking the BCC solid solutions for instance, the cluster is a rhombi-dodecahedron with a coordination number of 14 (CN14), and the cluster formula is expressed with the [rhombi-dodecahedron](glue atoms)$_x$. Among all the cluster-packing configurations, the cluster formula with $x = 1$ shows the highest cluster-packing density, which indeed interprets many commonly-used BCC industrial alloys [19]. So in the following, the [rhombi-dodecahedron](glue atoms)$_1$ formula will be considered to describe the lower limit of the Al content for the BCC stabilization in Al–Co–Cr–Fe–Ni multi-element alloy system.

In the Al–TM multi-element solid solution alloys, all the TMs can be treated as an averaged virtual element, M, that serves as the base solvent. Al is then regarded as the solute element, since Al has similarly strong interactions (negatively large ΔHs) with all TMs ($\Delta H_{Al–Co} = -19$ kJ/mol, $\Delta H_{Al–Cr} = -10$ kJ/mol, $\Delta H_{Al–Fe} = -11$ kJ/mol, and $\Delta H_{Al–Ni} = -22$ kJ/mol) [20]. Thus, an alloy series of $Al_xCoCrFeNi$ could be expressed as Al_xM_4 ($M = Co_{1/4}Cr_{1/4}Fe_{1/4}Ni_{1/4}$, an equi-molar mixing). Then, the cluster formula of the stable BCC solid solution in Al–TM systems can be expressed with the formula of $[Al–M_{14}](Al,M)_1$, where one Al solute atom takes the cluster center due to its negative ΔH with all the TMs, and extra Al should go to the glue site that is otherwise occupied by the average element M. The upper limit of the Al content in this formula is, therefore, $[Al–M_{14}]Al_1 = Al_{12.5}M_{87.5}$ (atomic percent, at.%), which actually corresponds to the beginning of the BCC phase formation, as evidenced in the alloy of $Al_{0.5}M_4$ ($Al_{11.1}M_{88.9}$ at.%) where the BCC phase begins to appear out of the FCC matrix [8]. The VEC value of 7.67 of this $[Al–M_{14}]Al_1$ is too high due to the high VEC ($VEC_M = 8.25$) of $M = Co_{1/4}Cr_{1/4}Fe_{1/4}Ni_{1/4}$ in comparison with the VEC of 6.87, the experimentally-determined upper VEC limit for the BCC single-phase zone [14]. There are two ways to decrease the VEC values, either by increasing the Al content or by adjusting the average element M. It was experimentally proved that upon further increasing the Al content, the mechanical properties of alloys would be deteriorated. For instance, the alloy, AlCoCrFeNi ($Al_{20}M_{80}$ at.%), exhibits a nearly

Fig. 2. SEM images of the suction-cast $Al_{0.7}CoCrFe_2Ni$ alloy. (a): low-magnification image; (b) and (c): magnified images of the indicated zones of '1' and '2' in (a), respectively.

limit of the single BCC phase zone), some residual FCC phase would be formed, which might contribute favorably to the ductility. It will be shown in the following that the designed alloy, $Al_{0.7}CoCrFe_2Ni$, exhibits a desired microstructure of a BCC matrix with cuboidal B2 coherent nanoprecipitates plus minor FCC residues, which renders the alloy with high tensile strength and good ductility at both room and elevated temperatures.

The $Al_{0.7}CoCrFe_2Ni$ ($Al_{6.4}Co_{19.6}Cr_{17.3}Fe_{37.2}Ni_{19.5}$ wt.%) alloy was prepared by means of arc melting and copper-mold suction-casting into ϕ6-mm rods under an argon atmosphere. The purities of the raw metals are 99.99% for Al, Co, Fe and Ni, and 99.9% for Cr. These alloy ingots were re-melted at least five times to ensure the chemical homogeneity before suction-casting. The phase constitution was identified using the BRUKER X-ray diffractometer (XRD) with the Cu K_α radiation ($\lambda = 0.15406$ nm). The microstructure was characterized by scanning electron microscopy (SEM, Zeiss Supra 55), after being etched in a solution of 5 g $FeCl_3 \cdot 6H_2O$ + 25 ml HCl + 25 ml C_2H_5OH, and by transmission electron microscopy (TEM, Philips Tecnai G^2). The TEM samples were prepared by twin-jet electro-polishing in a solution of 10% $HClO_4$ + 90% C_2H_5OH (volume fraction) at about −30 °C. Both uniaxial compressive and tensile tests were conducted on an 810 Material Test System (MTS) equipped with a heating furnace. The mechanical tests were performed at room temperature, 650 °C, and 700 °C with a strain rate of $2 * 10^{-4}$ /s. The cylindrical samples for compression have a size of ϕ3 * 6 mm, machined from the ϕ6 mm rods. The rod-shaped tensile samples have a gauge section of 3 mm in diameter and a length of 25 mm. The room-temperature properties were measured with a strain gauge. At least three specimens were tested under each condition.

The XRD result in Fig. 1 shows that the suction-cast alloy is mainly composed of the BCC solid solution, plus minor B2 ordered phase (characterized by a weak (100) diffraction peak) and residual FCC phase. The lattice constants of the BCC, B2, and FCC phases are calculated, being respectively $a_{BCC} = 0.2862$ nm, $a_{B2} = 0.2851$ nm, and $a_{FCC} = 0.3587$ nm. The dual-phase of (BCC + B2) exhibits a large columnar dendritic microstructure, and the FCC phase exists in the inter-dendritic regions, as shown in Fig. 2(a). Moreover, nanosized cuboidal B2 particles (dark ones in Fig. 2(b)) are uniformly precipitated on the BCC matrix, and the FCC phase has a sideplate microstructure with a lamellar spacing of about 200 nm (Fig. 2(c)). The selected-area electron diffraction (SAED) pattern of TEM verifies further that the dendrites are composed of BCC and B2 phases (Fig. 3(a)), where the cuboidal B2 particles have a size of about 50–100 nm and are embedded coherently in the disordered BCC matrix, seen in the dark-field TEM image (Fig. 3(a)) obtained by selecting one of the extra reflections (encircled in the SAED pattern). Thereof, the present alloy is characterized by cuboidal B2 nanoparticles in coherent precipitation from the BCC matrix, as well as minor FCC lamellae.

At room temperature, this alloy exhibits a combination of high strength and good ductility under both compression and tension cases. The tensile property parameters are yielding strength $\sigma_y = 866$ MPa, ultimate strength $\sigma_b = 1223$ MPa, and elongation to fracture $\delta = 7.9\%$, as shown in Fig. 4(a), being the engineering tensile stress-strain curves at room and elevated temperatures. In addition, the room-temperature compressive property is much better with $\sigma_y = 1166$ MPa, $\sigma_b = 1945$ MPa, and $\delta = 30.2\%$. More importantly, this alloy also possesses higher tensile strengths at elevated temperatures, with $\sigma_b = 468$ MPa at 650 °C, and $\sigma_b = 340$ MPa at 700 °C (Fig. 4(a)).
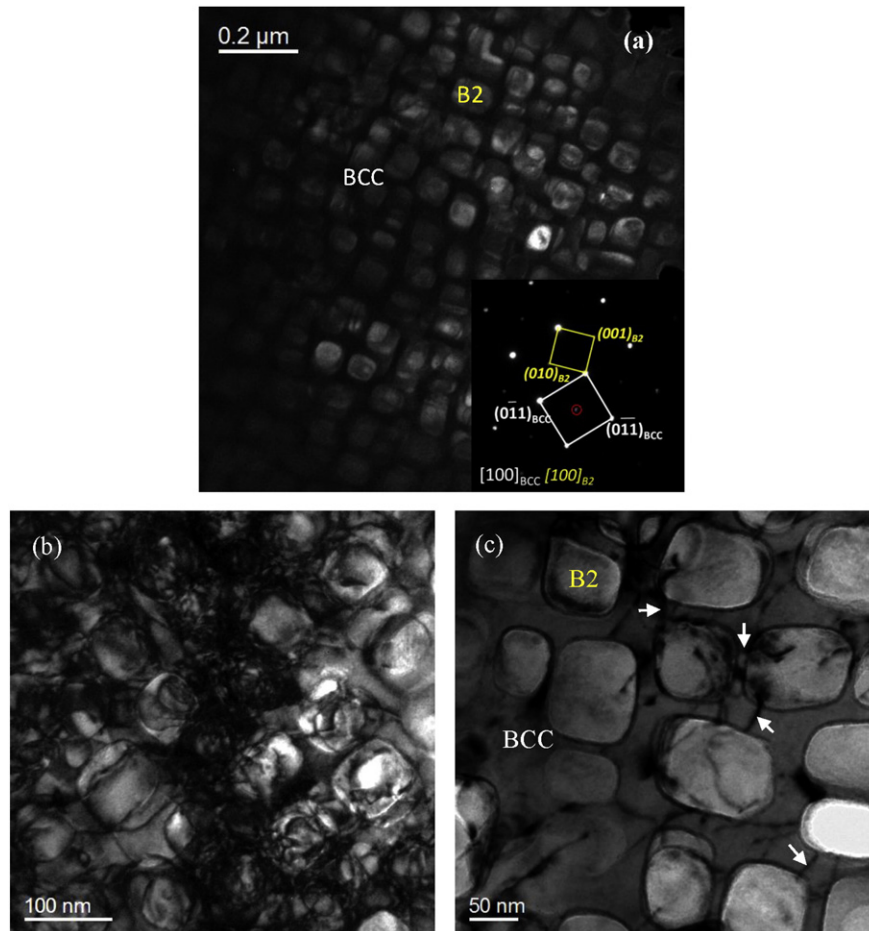

Fig. 3. TEM images and SAED patterns of the $Al_{0.7}CoCrFe_2Ni$ alloy. (a) dark-field image of BCC/B2 matrix before tension, and (b, c) bright-field images of BCC/B2 matrix after tension in which a large amount of dislocations are in the BCC phase.

Among the as-cast Al$_x$CoCrFeNi alloys, the FCC Al$_{0.3}$CoCrFeNi alloy has a good tensile plasticity but its ultimate tensile strength is below 350 MPa at room temperature [9]. While the spinodal-type BCC/B2 AlCoCrFeNi alloy is very brittle, where dislocations are practically absent, with a zero tensile ductility at room temperature and only 1.0% at 700 °C [11,21]. Upon the Cu addition, the AlCoCuCrFeNi becomes a dual-phase alloy with FCC plus BCC, but its tensile plasticity remains poor [22]. While the Al$_{0.5}$CoCuCrFeNi alloy can show both high tensile strength and good ductility after cold rolling, owing to a microstructure of cuboidal L1$_2$-γ′ precipitates embedded coherently in the FCC-γ matrix [10], which is responsible for the high strength and good ductility at both room and elevated temperatures [1]. The present Al$_{0.7}$CoCrFe$_2$Ni alloy exhibits a similar precipitation morphology but based on the BCC-based structure, i.e., nanosized cuboidal B2 precipitation in coherence with the BCC matrix. This kind of microstructure should be the result of a suitable lattice misfit ε [23] between the BCC and B2 phases, i.e., ε = 2 × (a$_{B2}$ − a$_{BCC}$) / (a$_{B2}$ + a$_{BCC}$) = −0.38%, within the range of −0.2 to −0.5% of Ni-based superalloys [1,24], which contributes to its high strength and good ductility. A large lattice misfit generally leads to a spinodal-type microstructure [11,12]. It was observed by TEM that a large amount of dislocations were induced in the cuboidal B2 plus BCC matrix after the tensile deformation at room temperature (Fig. 3(b, c)). Most of the dislocations are existed in the BCC phase and terminated at the BCC/B2 interfaces, as marked by arrows in Fig. 3(c), which is also quite similar to the dislocation distribution in γ/γ′-type superalloys [1,24], indicating that the present alloy Al$_{0.7}$CoCrFe$_2$Ni might be used at high temperatures.

For the coherent-precipitate strengthening, the dislocation shear mechanism plays a dominant role, in which the increment in yielding strength (Δσ$_{CS}$) results primarily from the contribution of coherency strengthening [1,13,25,26]. The equation to calculate Δσ$_{CS}$ is Gεc [25,26], where M = 2.73 for BCC structure (Tailor factor), α$_ε$ = 2.6 (a constant), ε$_c$ = 2ε/3, the constrained lattice misfit. G, b, r, and f are respectively the shear modulus, the Burgers vector, the average radius and the volume fraction of the precipitates. Thus, the strength increment, Δσ$_{CS}$ = 1129 MPa, can be calculated using G = 83 GPa (for α-Fe), b = √3 × a$_{BCC}$ / 2 = 0.2478 nm, r = 70 nm, and f = 0.4. The Δσ$_{CS}$ value is larger than the measured tensile yield strength of σ$_y$ = 866 MPa, but is close to the compressive σ$_y$ = 1166 MPa, which may be caused by the presence of soft inter-dendrite FCC lamellae (Fig. 2). It should be pointed out that this large Δσ$_{CS}$ is closely related to r, f, and especially ε. Therefore, controlling a reasonable ε is of most importance to realize a cuboid-coherent precipitation. Moreover, fixing f = 0.4, the largest yielding strength increment could be reached when Δσ$_{CS}$ = Δσ$_{orowan}$ at a critical precipitate radius r$_0$, ignoring the contribution from the modulus mismatch. The strength increment Δσ$_{orowan}$ = M ·[0.4Gb/(π√(1−ν))] · [ln(2√(2/3) · r/b)/λ$_p$] results from the Orowan dislocation bypass mechanism [25], where ν = 0.3 is the Poisson ratio, and λ$_p$ = 2√(2/3)r(√(π/4f)−1) is the distance between precipitates. Thereof, the calculated critical r$_0$ of the B2 cuboids is about 71 nm, consistent with the experimental average value of 70 nm, which indicates that the largest strength increment is achieved by this kind of microstructure.

Fig. 4(b) compares the ultimate tensile strength σ$_b$ at different temperatures of the present alloy Al$_{0.7}$CoCrFe$_2$Ni with those of some reported Al–TM multi-element alloys. It can be seen that the tensile properties (strength and ductility) of the present BCC-based alloy are better than all the above mentioned Al–TM BCC-based alloys due to its cuboid-coherent BCC/B2 microstructure. Its room-temperature properties are comparable with the as-rolled FCC-based Al$_{0.5}$CoCrFeNiCu alloy but are higher than those of the annealed alloy, as shown in Fig. 4(b). In addition, the latter becomes brittle above 600 °C due to a non-coherent BCC phase precipitation [27]. More importantly, at the elevated temperature of 700 °C, the present alloy has a much higher strength (σ$_b$ = 340 MPa) than that of the latter in the rolled state (σ$_b$ = 203 MPa).
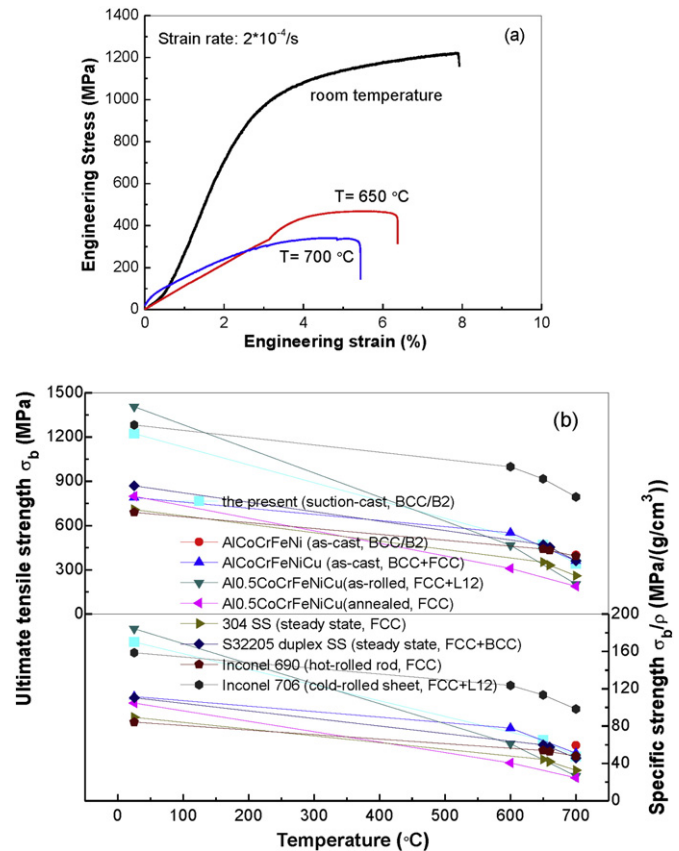

Fig. 4. Engineering tensile stress-strain curves of the Al$_{0.7}$CoCrFe$_2$Ni alloy at different temperatures (a), and comparisons of the ultimate tensile strength σ$_b$ (including the specific strength σ$_b$/ρ) of the present Al$_{0.7}$CoCrFe$_2$Ni alloy with those of typical Al–TM multi-principal-element alloys and common engineering alloys.

Four common engineering alloys are also compared in Fig. 4(b), including 304 stainless steel (0Cr18Ni9 in weight percent form, FCC), S32205 duplex stainless steel (00Cr22Ni5Mo3N, BCC plus FCC), Inconel 706 (Ni-base superalloy, 00Fe38Cr16Nb3Ti1.8, L1$_2$ coherently-enhanced FCC), and Inconel 690 (Ni-base superalloy, 00Cr28Fe10, FCC). Obviously, the room-temperature σ$_b$ of the present Al$_{0.7}$CoCrFe$_2$Ni alloy is much higher than those of 304 and S32205 in the steady state (ASTM Standard E21-92) [28]. At elevated temperatures, the σ$_b$ of the present alloy reaches that of S32205 and is higher than that of 304. As far as the Ni-base superalloys are concerned, the present alloy has a comparable room-temperature σ$_b$ with Inconel 706 [29]. At high temperatures, the strength of the present alloy is lower than that of Inconel 706 but reaches the level of Inconel 690 [30]. In terms of the specific strength, σ$_b$/ρ, shown in Fig. 4(b), the present alloy Al$_{0.7}$CoCrFe$_2$Ni belongs to the higher-strength category at all temperatures among these different kinds of alloys compared. Therefore, it can be anticipated that this superalloy-like BCC-based Al$_{0.7}$CoCrFe$_2$Ni alloy is potentially useful as a high-temperature structural material.

In summary, a cluster formula of [Al–M$_{14}$]Al$_1$ issued from the cluster-plus-glue-atom model is applied to design a multi-principal-element alloy, where the solvent M is averaged from all transition metals, M = Co$_{1/5}$Cr$_{1/5}$Fe$_{2/5}$Ni$_{1/5}$. The designed alloy, Al$_{0.7}$CoCrFe$_2$Ni (molar ratio), exhibits prominent tensile properties at both room temperature (σ$_b$ = 1223 MPa and δ = 7.9%) and elevated temperatures (e.g. σ$_b$ = 468 MPa at 650 °C), which are far superior to all known BCC-based Al-transition metal multi-principal-element alloys and are comparable to Ni-based superalloys such as Inconel series, and stainless steels such as S32205. The excellent performance of high strength and good ductility is closely related to a superalloy-like microstructure

characterized by cuboidal B2 nanoparticles embedded coherently in the BCC matrix.

References

[1] R.C. Reed, The Superalloys: Fundamentals and Applications, Cambridge University Press, New York, USA, 2006.
[2] Z.K. Teng, C.T. Liu, G. Ghosh, P.K. Liaw, M.E. Fine, Intermetallics 18 (2010) 1437–1443.
[3] J.W. Yeh, S.K. Chen, S.J. Lin, J.Y. Gan, T.S. Chin, T.T. Shun, C.H. Tsau, S.Y. Chang, Adv. Eng. Mater. 6 (2004) 299–303.
[4] Y. Zhang, T.T. Zuo, Z. Tang, M.C. Gao, K.A. Dahmen, P.K. Liaw, Z.P. Lu, Prog. Mater. Sci. 61 (2014) 1–93.
[5] O.N. Senkov, J.D. Miller, D.B. Miracle, C. Woodward, Nat. Commun. 6 (2015) 7529.
[6] B. Gludovatz, A. Hohenwarter, D. Catoor, E.H. Chang, E.P. George, R.O. Ritchie, Science 345 (2014) 1153–1158.
[7] M.H. Tsai, J.W. Yeh, Mater. Res. Lett. 2 (2014) 107–123.
[8] Y.F. Kao, T.J. Chen, S.K. Chen, J.W. Yeh, J. Alloys Compd. 488 (2009) 57–64.
[9] T.T. Shun, Y.C. Du, J. Alloys Compd. 479 (2009) 157–160.
[10] M.A. Hemphill, T. Yuan, G.Y. Wang, J.W. Yeh, C.W. Tsai, A. Chuang, P.K. Liaw, Acta Mater. 60 (2012) 5723–5734.
[11] T. Zhi, T. Yuan, C.W. Tsai, J.W. Yeh, C.D. Lundin, P.K. Liaw, Acta Mater. 99 (2015) 247–258.
[12] W.R. Wang, W.L. Wang, J.W. Yeh, J. Alloys Compd. 589 (2014) 143–152.
[13] J.Y. He, H. Wang, H.L. Huang, X.D. Xu, M.W. Chen, Y. Wu, X.J. Liu, T.G. Nieh, K. An, Z.P. Lu, Acta Mater. 102 (2016) 187–196.
[14] S. Guo, C. Ng, J. Lu, C.T. Liu, J. Appl. Phys. 109 (2011) 103505.
[15] J.M. Cowley, Phys. Rev. 120 (1960) 1648–1657.
[16] P. Singh, A.V. Smirnov, D.D. Johnson, Phys. Rev. B 91 (2015) 224204.
[17] L.J. Santodonato, Y. Zhang, M. Feggenson, C.M. Parish, M.C. Gao, R.J.K. Weber, J.C. Neuefeind, Z. Tang, P.K. Liaw, Nat. Commun. 6 (2015) 5964.
[18] H.L. Hong, Q. Wang, C. Dong, P.K. Liaw, Sci. Rep. 4 (2014) 7065.
[19] C. Pang, B.B. Jiang, Y. Shi, Q. Wang, C. Dong, J. Alloys Compd. 652 (2015) 63–69.
[20] A. Takeuchi, A. Inoue, Mater. Trans. 41 (2000) 1372–1378.
[21] Y.P. Wang, B.S. Li, M.X. Ren, C. Yang, H.Z. Fu, Mater. Sci. Eng. A 491 (2008) 154–158.
[22] A.V. Kuznetsov, D.G. Shaysultanov, N.D. Stepanov, G.A. Salishchev, O.N. Senkov, Mater. Sci. Eng. A 533 (2012) 107–118.
[23] P.W. Voorhees, G.B. Mcfadden, W.C. Johnson, Acta Metall. Mater. 40 (1992) 2979–2992.
[24] J.X. Zhang, J.C. Wang, H. Harada, Y. Koizumi, Acta Mater. 53 (2005) 4623–4633.
[25] T.H. Courtney, Mechanical Behavior of Materials, second ed. Waveland, Long Grove, 2005.
[26] A.J. Ardell, Metall. Trans. A 16 (1985) 2131–2165.
[27] C.W. Tsai, M.H. Tsai, J.W. Yeh, C.C. Yang, J. Alloys Compd. 490 (2010) 160–165.
[28] J. Chen, B. Young, Eng. Struct. 28 (2006) 229–239.
[29] http://www.specialmetals.com/assets/documents/alloys/inconel/inconel-alloy-706.pdf.
[30] http://www.specialmetals.com/assets/documents/alloys/inconel/inconel-alloy-690.pdf.